JOURNAL OF SOLID STATE CHEMISTRY 107, 460–470 (1993)

Crystal Structure and Ionic Conductivity of a Layered Perovskite, $AgLaNb_2O_7$

M. SATO,* J. WATANABE, AND K. UEMATSU

Department of Material and Chemical Engineering, Faculty of Engineering, Niigata University, Niigata 950-21, Japan

Received July 2, 1992; in revised form April 7, 1993; accepted April 8, 1993

A layered perovskite compound, $AgLaNb_2O_7$, was newly prepared by an ion-exchange reaction. The compound showed an irreversible phase transition at 330°C. The crystal structures of low-temperature and high-temperature phases were determined by the Rietveld analysis for the X-ray powder diffraction patterns. The unit cell is tetragonal with a = 7.7757(4) Å, c = 42.587(2) Å, and Z = 16 with $I4_1/acd$ space group for the β-phase (low-temperature phase), and tetragonal with a = 3.8996(9) Å, c = 21.688(5) Å, and Z = 2 with $I4/mmm$ space group for the α-phase (high-temperature phase). The main structural difference between the two phases is due to the arrangement of silver ions located in the interlayer of the perovskite layers. The ionic conductivity attributed to the interlayer silver ions was observed, but its magnitude was rather small, $\sim 10^{-5}$ S cm^{-1} at 25°C. An abrupt decrease in the ionic conductivity was observed at the phase transition temperature. This behavior is discussed on the basis of the crystal structures of the two phases.

Introduction

Recently, much attention has been attracted to layered perovskite compounds such as $K_2La_2Ti_3O_{10}$ and $KCa_2Nb_3O_{10}$, which are two of the members of the Ruddlesden–Popper phase (*1*), because of their potential ability for ion-exchange in the alkali ion sites (*2–6*), intercalation reactions (*7, 8*), and photocatalytic reactions (*9*). Many of their ion-exchanged forms with sodium, lithium, and other protons, which are located in the interlayer sandwiched by the perovskite layers, can be prepared once by using a soft chemistry, but have never been obtained by a solid state reaction at high temperatures. Such ion-exchanged compounds are thought to be virtually thermodynamically metastable phases at ambient temperature. From the perspective of synthesizing new materials, the ion-exchange reaction involved in these compounds is also of particular interest.

The authors have already determined the structures of $M LaNb_2O_7$ (M = K, Na, Li, and H), which are other materials exhibiting ion-exchange reactions, by using the Rietveld method and have discussed the relationship between the structure and the ionic conduction coming from the ions located in the interlayer (*10–12*). During the investigations of these compounds, we have recently found that the silver exchanged phase, $AgLaNb_2O_7$, can be newly synthesized by reaction with $AgNO_3$ molten salt. In this paper we describe the structure of this compound, and in addition discuss its ionic conductivity which is relatively higher at room temperature than those of the sodium and lithium phases.

Experimental

$AgLaNb_2O_7$ was prepared by the ion-exchange reaction of $RbLaNb_2O_7$ powder with a molten salt of $AgNO_3$.

* To whom correspondence should be addressed.

0022-4596/93 $5.00

The starting materials for the preparation of $RbLaNb_2O_7$ were Rb_2CO_3, La_2O_3, and Nb_2O_5. The preparation of $RbLaNb_2O_7$ was carried out by using a method similar to that in the previous study (*10*).

The ion-exchange reaction was done by adding the ground $RbLaNb_2O_7$ powder to a molten salt of $AgNO_3$ at 230°C for 24 hr. The solid product obtained was washed with distilled water and dried at 110°C for 24 hr. The completion of the ion-exchange reaction was confirmed by X-ray powder diffraction and X-ray fluorescence analyses.

Thermogravimetric analysis (TGA) and differential thermal analysis (DTA) were carried out using a Mac Science thermal analyzer system 001 at a heating rate of 5°C min^{-1}.

The X-ray powder diffraction patterns were obtained at 25, 350, and 700°C, using a Rigaku RAD-rA diffractometer equipped with a high-temperature furnace attachment. The Cu $K\alpha$ radiation used was monochromated by a curved-crystal graphite. The data were collected on thoroughly ground powders by a step-scanning mode in a 2θ range of 5 to 100° with a step width of 0.04° and a step time of 4 sec. The powder patterns obtained were analyzed by the Rietveld method, using the RIETAN profile refinement program (*13*) on an ACOS 2010 computer at Niigata University.

The specimen for the conductivity measurement was prepared by pressing the powder sample into a compact disc at a pressure of 4 tons cm^{-2}. The typical dimensions of the discs were 10 mm in diameter and about 1.0 mm thick, and both sides of the disc were coated with an evaporated silver film. The conductivities were determined by the complex impedance diagrams obtained by using alternating currents with the frequencies between 40 and 100 kHz, using a Hioki 3520 Hi Tester at the temperature range from 25 to 500°C in dry air.

Results and Discussion

Structural Analysis

The thermal stability of $AgLaNb_2O_7$ obtained was examined by TGA and DTA. The results are shown in Fig. 1. No weight loss is observed until 650°C, followed by large weight loss due to the thermal decomposition. Powder X-ray diffraction pattern obtained after heating at 750°C shows the reflection peaks of $LaNbO_4$ as a major decomposition product. A small and broad exothermic peak is found at 330°C in the DTA curve, implying some kind of phase transition because of a lack of weight loss at this temperature. In order to clarify this behavior, high-temperature X-ray diffraction measurement was done at 350°C which is slightly higher than the temperature for the exothermic peak. The powder X-ray diffraction pattern obtained at 350°C is shown in Fig. 2 together with that at room temperature. Apparently, one can distinguish some new reflection peaks in the room-temperature pattern in addition to intensive reflections commonly observed in the two patterns. Further DTA and X-ray diffraction analyses indicated that this phase transition is irreversible. Therefore, the data for the Rietveld analysis of the high-temperature phase were collected at room temperature after heating the sample at 350°C. In order to simplify identification of the two polymorphs, we label the low-temperature phase the β-phase and the high temperature phase the α-phase in the following sections.

The indexing of the powder patterns obtained for the two phases was examined with the aid of the computer program CELL (*14*). All of the reflections obtained for the α-phase could be easily assigned as a tetragonal symmetry with the cell parameters approximately equal to a = 3.90 Å and c = 21.68 Å. The reflection condition found for this phase was $h + k + l = 2n$ for hkl reflections, leading to the I^{***}-type space groups (*15*), i.e., the eight space groups $I4$, $I\bar{4}$, $I4/m$, $I422$, $I4mm$, $I\bar{4}m2$, $I\bar{4}2m$, and $I4/mmm$. On the other hand, the pattern for the β-phase is more complicated. It is, however, very interesting that the reflections, except for some peaks (as indicated by the arrows in Fig. 2a), could also be assigned as a tetragonal symmetry with almost

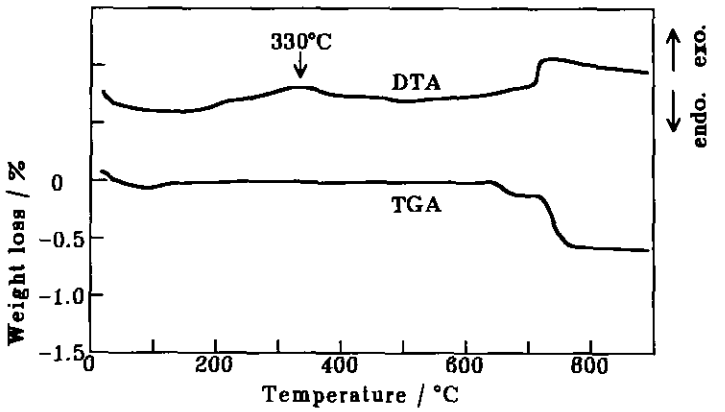

FIG. 1. Thermogravimetric and differential thermal curves for $AgLaNb_2O_7$.

the same cell dimensions as those for the α-phase. This finding means that the β-phase has essentially similar crystal structure to that for the α-phase even though its crystal symmetry becomes lower. Therefore, we have examined the indexing for the β-phase by using the cell parameters with larger values than those found in the α-phase. As a result, all of the reflections for the β-phase could be completely assigned to another tetragonal symmetry with the cell parameters approximately equal to 7.78 Å and 42.64 Å on the basis of the $I4_1/acd$ space group. It is obvious that this phase has cell

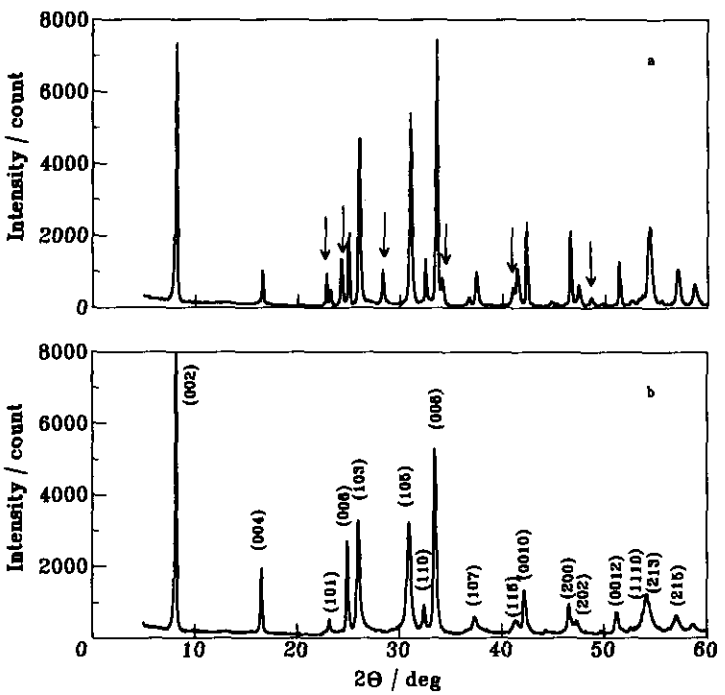

FIG. 2. Powder X-ray diffraction patterns for β-phase (a) and α-phase (b) of $AgLaNb_2O_7$. The reflections indicated by arrows in (a) are reflections which are absent in (b).

dimensions twice as large as those for the α-phase.

The cell parameters obtained for the α-phase are quite compatible with those for the anhydrous Na-exchanged compound, $NaLaNb_2O_7$, e.g., $a = 3.902$ Å and $c = 21.182$ Å (*11*). This compound has a layered perovskite structure where adjacent perovskite layers are stacked with a displacement by translating by $\frac{1}{2}$ along the [110] direction, Na ions being located in a tetrahedral site in the interlayer. Since the β-phase has cell parameters almost twice as large as those of $NaLaNb_2O_7$, the basic structure of the β-phase as well as of the α-phase is considered to be similar to that of this compound. An initial structural model for the β-phase was embodied after some trials on the basis of the structure of anhydrous $NaLaNb_2O_7$. For the Rietveld refinement, an extended pseudo-Voigt function and an asymmetric function described in the literature (*16*) were chosen to generate the line shape of the diffraction peaks. In the early refinement stage, it was found that the threshold of the reflection peak observed at $2\theta = 8.3°$ in the powder pattern deviates greatly from the calculated peak profile due to the asymmetric effect of the peak shape at this low-2θ region. Therefore, this reflection peak was eliminated from further refinements. In the final refinement stage, fourteen positional parameters, isotropic thermal parameters for all atoms, and a scale factor were refined. A preferred orientation correction (*17*) was made because this phase showed strong (001) preferred orientation due to its layered structure. On the other hand, for the α-phase, the typical coordinates of the anhydrous $NaLaNb_2O_7$ structure with *I4/mmm* space group (*11*) were used in the initial refinement stage. Finally, a preferred orientation correction was also made for this phase. In Table I are given the data collection conditions, some crystallographic data, and the final reliable factors achieved for both phases. The positional parameters and the selected interatomic distances and angles are listed in Tables II–V.

Description of the Structure

Although the crystallinity of the β-phase became relatively poor compared with the mother material of $RbLaNb_2O_7$, the *R*-factors for the α-phase were reasonably converged at the final refinement stage. As shown in Fig. 2, one can notice much poorer crystallinity for the α-phase than for the β-phase, e.g., the reflection peaks in the α-phase have significantly larger full width at half-maximum (FWHM) values as well as background intensities. In addition, asymmetric line broadening was also observed in some reflections of the α-phase, for example, the (103) and (105) reflections. Such poor crystallinity could give the fairly high *R*-factors finally obtained for the α-phase, even though the refinement was done by considering an asymmetric effect for the peak shape. One of the possible reasons for the poor crystallinity may be due to the case where the α-phase actually has a lower crystal symmetry, for example, an orthorhombic symmetry or a longer *a*-axis (doubling of the *a*-axis) in a tetragonal symmetry. In the further Rietveld refinements on the basis of these assumptions, it was found that no structural models based on such possibilities gave solutions with physical meanings as well as more reliable *R*-factors than those listed in Table I. Therefore, it is possible to conclude that the results obtained for the α-phase are substantially acceptable although the results do not lead to an accurate structure.

The proposed crystal structures for both phases are shown in Figs. 3 and 4. The main frame in the crystal structure of the α-phase is exactly the same as that of $NaLaNb_2O_7$ and $LiLaNb_2O_7$ reported previously (*11, 12*). The structure of the β-phase has basically the same layered structure sequence, but has about eight times as large a cell volume as those of the α-phase due to the lower symmetry. Both structures are characterized as nearly the two-dimensional framework of the $LaNb_2O_7$ layer perpendicular to the *c*-axis. The adjacent double-perovskite layers are stacked on top of each other with

TABLE I

DATA COLLECTION CONDITIONS, CRYSTALLOGRAPHIC DATA, AND RELIABLE FACTORS FOR $AgLaNb_2O_7$

	β-phase	α-phase
Radiation	Cu $K\alpha$	Cu $K\alpha$
2θ range (°)	10–100	10–100
Step scan increment (2θ°)	0.04	0.04
Count time (sec/step)	4	4
Measuring temp. (°C)	25	25 (after heating at 350°C)
Space group	$I4_1/acd$ (No. 142)	$I4/mm$ (No. 139)
a (Å)	7.7757(4)	3.8996(9)
c (Å)	42.587(2)	21.688(5)
Volume (Å^3)	2574.9	329.8
Z	16	2
Calculated density (g/cm^3)	5.619	5.483
No. of structural parameters refined	24	11
No. of profile parameters refined	16	16
No. of reflections	663	150
Reliable factors[a]		
R_{wp}	0.1350	0.1877
R_p	0.1138	0.1449
R_I	0.0426	0.0767
R_F	0.0187	0.0348

[a] Defined as follows: $R_{wp} = [(\sum w_i[Y_{obs} - Y_{cal}]^2)/(\sum w_i[Y_{obs}]^2)]^{1/2}$, $R_p = (\sum |Y_{obs} - Y_{cal}|)/(\sum Y_{obs})$, $R_I = (\sum |I_{obs} - I_{cal}|)/(\sum I_{obs})$, $R_F = (\sum |[I_{obs}]^{1/2} - [I_{cal}]^{1/2}|)/(\sum [I_{obs}]^{1/2})$.

the displacement by translating the perovskite layer by $\frac{1}{4}$ for the β-phase and $\frac{1}{2}$ for the α-phase along the [110] direction. The doubling of the a-axis found in the β-phase is considered to result from the deformation of the NbO_6 octahedron and the twisting in the linkage of the corner-sharing NbO_6 octahedra along the c-axis as shown in Fig. 5. Owing to the poor crystallinity of not only the α-phase but also the β-phase, the accuracy of the positional and isotropic thermal parameters refined was rather poor (rather

TABLE II

ATOMIC POSITIONS AND ISOTROPIC TEMPERATURE FACTORS FOR β-PHASE OF $AgLaNb_2O_7$ (a = 7.7757(4)Å, c = 42.587(2)Å, and Z = 16 for $I4_1/acd$ WITH SECOND SETTING)

Atom	Site[a]	g[b]	x	y	z	B(Å^2)
Ag	16f	1.0	0.256(2)	0.506(2)	0.125	2.6(2)
La	16c	1.0	0.0	0.0	0.0	0.4(1)
Nb	32g	1.0	0.235(1)	0.257(2)	0.052(1)	0.1(16)
O(1)	16e	1.0	0.054(11)	0.0	0.25	2.8(20)
O(2)	16d	1.0	0.0	0.25	0.046(2)	0.9(34)
O(3)	16d	1.0	0.0	0.25	0.459(2)	0.1(26)
O(4)	32g	1.0	0.291(7)	0.027(11)	0.044(1)	0.5(13)
O(5)	32g	1.0	0.233(14)	0.243(16)	0.090(1)	1.0(10)

[a] Multiplicity and Wyckoff notation.
[b] Site occupation factor.

TABLE III

ATOMIC POSITIONS AND ISOTROPIC TEMPERATURE FACTORS FOR α-PHASE OF $AgLaNb_2O_7$ (a = 3.8940(5)Å, c = 21.357(3)Å, and Z = 2 for $I4_1/mmm$)

Atom	Site[a]	g[b]	x	y	z	B(Å^2)
Ag	4d	0.5	0.0	0.5	0.25	4.6(10)
La	2a	1.0	0.0	0.0	0.0	1.3(7)
Nb	4e	1.0	0.0	0.0	0.395(1)	0.8(5)
O(1)	8g	1.0	0.0	0.5	0.083(2)	4.3(22)
O(2)	4e	1.0	0.0	0.0	0.312(6)	10.6(47)
O(3)	2b	1.0	0.0	0.0	0.5	14.5(95)

[a] Multiplicity and Wyckoff notation.
[b] Site occupation factor.

high esd values were obtained), especially for the case of oxygen atoms which have relatively low atomic scattering factors in the X-ray diffraction measurement. The isotropic thermal parameters of the Ag atoms located in the interlayer for both phases are also fairly high, probably due to the thermal vibration mode restricted within the interlayer. This may again result in ambiguity for the position of the oxygen atoms toward the interlayer space, e.g., O(5) for the β-phase and O(2) for the α-phase. Nevertheless, the positional information such as bond lengths and polyhedra distortions can be considered interesting. As shown in Fig. 6, the NbO_6 octahedron in the β-phase is remarkably distorted from its ideal form, involving three kinds of Nb–O bond distances: e.g., a highly shortened bond (1.64 Å) toward the interlayer, four normal bonds (range 1.85–2.14 Å) linked within the perovskite layer, and a long bond (2.30 Å) located on the opposite side from the shortened bond. Such bond characters are also true for the α-phase, which has bond distances of 1.75, 2.00, and 2.24 Å corresponding, respectively, to the above three kinds of bondlength, but the distortion of NbO_6 seems to be fairly relaxed in this phase since the shortened bond becomes longer. Figure 7 shows the coordination around a silver atom and the linking sequence of Ag-polyhedra projected along the [001] direction. There exist some structural differences concerning the location of the silver atoms in the interlayer between the two phases. In both phases, each silver atom is surrounded by four oxygens, forming AgO_4 tetrahedra. The AgO_4 tetrahedron of the α-phase is an almost perfect tetrahedron with four Ag–O bonds of identical length and with two kinds of O–Ag–O angles (108.8° and 110.7°) nearly equal to the 109.5° angle for a perfect tetrahedron. On the other hand, the situation for the β-phase is quite different, where the coordination of the silver atom is a somewhat distorted tetrahedral coordination with the Ag–O distances and O–Ag–O angles both ranging to some extent. In addition to the above features, the locations of the silver atoms in the β-phase are considerably different from those in the α-phase; e.g., the tetrahedra neighboring by edge-sharing with the AgO_4 tetrahedra are all vacant, while all of the tetrahedra in the α-phase contain the silver atom with 50% occupancy. Since the arrangement of the silver atoms found in the α-phase is more favorable with regard to the entropy contribution, it may be concluded that the phase transition from β-phase to α-phase is a sort of order–disorder phase transition with respect to the rearrangement of the interlayer atoms.

The tetrahedral AgO_4 coordination found in $AgLaNb_2O_7$ is relatively rare in the normal oxides containing silver. Due to its electronic configuration, silver atoms have a strong covalent bond character in oxides.

TABLE IV

BOND DISTANCES (Å) AND ANGLES (°) FOR β-PHASE OF $AgLaNb_2O_7$

Distance	
Ag–O(5)	2.51(10) × 2
Ag–O(5)^{v}	2.34(9) × 2
La–O(1)^{ii}	3.06(6) × 2
La–O(1)^{vi}	2.47(5) × 2
La–O(2)	2.78(6) × 2
La–O(3)^{iv}	2.60(6) × 2
La–O(4)	2.95(5) × 2
La–O(4)^{iii}	2.49(4) × 2
Nb–O(1)^{vi}	2.30(1)
Nb–O(2)	1.85(1)
Nb–O(3)^{i}	2.11(2)
Nb–O(4)	1.87(8)
Nb–O(4)^{v}	2.14(8)
Nb–O(5)	1.62(2)
Angle	
O(5)–Ag–O(5)^{v}	106.5(9)
O(5)–Ag–O(5)^{vii}	115.9(46)
O(5)–Ag–O(5)^{ix}	102.7(46)
O(5)–Ag–O(5)^{viii}	109.2(46)
O(5)–Nb–O(1)^{vi}	163.9(48)
O(5)–Nb–O(2)	97.2(41)
O(5)–Nb–O(3)^{i}	104.7(40)
O(5)–Nb–O(4)	97.8(44)
O(5)–Nb–O(4)^{v}	103.8(44)
O(4)–Nb–O(1)^{vi}	66.1(22)
O(4)–Nb–O(2)	99.6(21)
O(4)–Nb–O(3)^{i}	72.6(21)
O(4)–Nb–O(4)^{v}	157.1(13)
O(3)^{i}–Nb–O(1)^{vi}	72.9(24)
O(3)^{i}–Nb–O(2)	157.3(18)
O(3)^{i}–Nb–O(4)^{v}	94.6(17)
O(2)–Nb–O(4)^{v}	94.8(17)
O(2)–Nb–O(1)^{vi}	84.4(26)
O(1)^{vi}–Nb–O(4)^{v}	92.1(23)
Nb–O(1)^{vi}–Nb–^{viii}	155.9(43)

Symmetry codes: (none) x, y, z; (i) $\frac{1}{2} - x$, $\frac{1}{2} - y$, $\frac{1}{2} - z$; (ii) $\frac{1}{4} + y$, $-\frac{1}{4} - x$, $\frac{1}{4} - z$; (iii) $\frac{1}{2} - x$, y, $-z$; (iv) x, $-y$, $\frac{1}{2} - z$; (v) $\frac{1}{2} - x$, $\frac{1}{2} + y$, z; (vi) $\frac{1}{4} - y$, $\frac{1}{4} - x$, $\frac{1}{4} - z$; (vii) $\frac{1}{4} + y$, $\frac{3}{4} - x$, $\frac{1}{4} - z$; (viii) $\frac{1}{2} - x$, y, $-z$; (ix) $-\frac{1}{4} + y$, $\frac{1}{4} + x$, $\frac{1}{4} - z$.

For example, AgO contains two kinds of oxidation states of silver atoms with equal proportions: one is linear-coordinated Ag(I) due to the formation of *sp* hybridization and the other is approximately square-planar coordinated Ag(III) due to the formation of dsp^2 hybridization (*18*, *19*). These features are also encountered in $AgCrO_2$ (*20*) and Ag_2FeO_2 (*21*). In such silver oxides, the distance of the Ag–O bond is usually in the range 2.07–2.18 Å for Ag(I) and 2.02–2.04 Å for Ag(III). Therefore, it is expected that such oxides will be electronic conductors if possible. On the other hand, tetrahedral coordination of the silver atom is sometimes stabilized in an interstices site produced by the packing of large anions such as MoO_4^- and CrO_4^{2-} in $NaAgMoO_4$–II (*22*) and Ag_2CrO_4 (*23*), respectively, which seems to have a strong ionic bond character. It is likely that in these oxides the silver atom exists as an Ag^+ ion rather than as an Ag(I) atom with sp^3 hybridization. The situation of $AgLaNb_2O_7$ is considered to be this type

TABLE V

BOND DISTANCES (Å) AND ANGLES (°) FOR α-PHASE OF $AgLaNb_2O_7$

Distance	
Ag–O(2)	2.36(7) × 4
Ag–Ag^{i}	2.75(1)
La–O(1)	2.63(3) × 4
La^{ii}–O(3)	2.75(1) × 8
Nb–O(1)^{i}	2.00(1) × 4
Nb–O(2)	1.75(12)
Nb–O(3)	2.24(1)
Angle	
O(2)–Ag–O(2)^{i}	108.8(25)
O(2)–Ag–O(2)^{iii}	110.7(51)
O(2)–Nb–O(1)^{i}	103.4(16)
O(3)–Nb–O(1)^{i}	76.5(16)

Symmetry codes: (none) x, y, z; (i) $\frac{1}{2} - x$, $\frac{1}{2} - y$, $\frac{1}{2} - z$; (ii) $\frac{1}{2} + x$, $\frac{1}{2} + y$, $\frac{1}{2} + z$; (iii) x, $1 + y$, z.

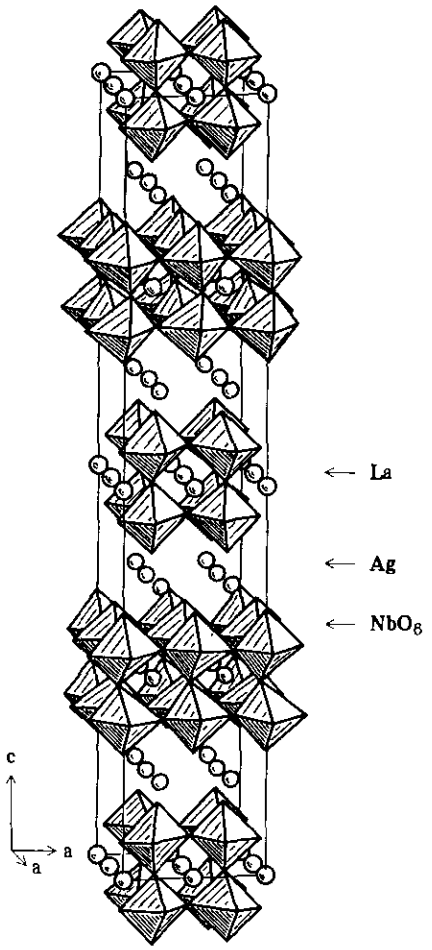

FIG. 3. Crystal structure for the β-phase of Ag $LaNb_2O_7$.

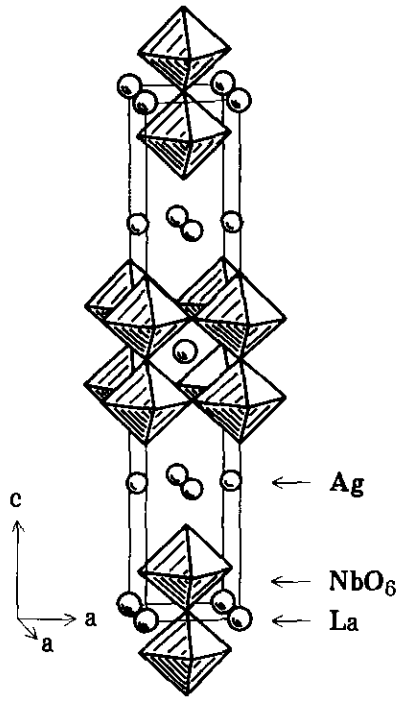

FIG. 4. Crystal structure for the α-phase of Ag $LaNb_2O_7$.

of case, where the $LaNb_2O_7$ unit may be regarded as a sort of oxo anion. Since Ag $LaNb_2O_7$ can only be produced by ion-exchange reaction, this compound should be a substantially metastable phase in the view of thermodynamics. It should be reasonable for silver ions in the β-phase to be located in the interlayer site in such a manner as to take a position with the most suitable space for Ag^+ in accordance with its ionic radius, and then to transform to the α-phase accompanied by the rearrangement of silver atoms, which is energetically more favorable at high temperatures. As a result, it seems that the silver atom has a strong ionic bond character in this compound, in spite of its tetrahedral coordination which is often established due to the covalent sp^3 hybridization. This consideration can be supported by the fact of relatively large Ag–O distances (ranging from 2.34 to 2.51 Å for the β-phase and 2.36 Å for the α-phase),

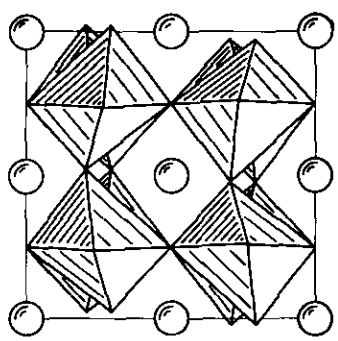

FIG. 5. The $LaNb_2O_7$ perovskite layer for the β-phase of $AgLaNb_2O_7$ projected along the [001] direction.

quite compatible with those found in $NaAgMoO_4$ (range 2.25–2.55 Å) (*22*).

Ionic Conduction Behavior

The compact disc sample of the β-phase was used as a starting material for the electrical conductivity measurements. In order to clarify the type of electrical conductivity of $AgLaNb_2O_7$, we have first done the preliminary measurement of a direct current polarization by using a reversible electrode of evaporated silver and an ion-blocking electrode of carbon. Analyzing the results by means of the Wagner method (*24*), it was found that the transport numbers for electron and hole conduction are both quite small, less than 10^{-3}, at temperatures of 25 and 100°C. The electrical conductivity was obtained from the Cole–Cole plot analysis by AC impedance measurement. Figure 8 shows the temperature dependence of conductivity for both temperature increasing and decreasing directions. Taking into account the results of the measurement of the transport number, the conductivities shown in the figure should correspond mostly to the ionic conduction attributed to silver ions located in the interlayer. An almost linear correlation is observed in the $\log(\sigma)$ vs $1/T$ plot in the temperature region from near room temperature to 300°C for the temperature increasing direction. However, an abrupt decrease in the conductivity is found at about 350°C. In the temperature decreasing direction, the conductivities decrease linearly down to 150°C with almost the same slope as that for the temperature increasing direction, but their magnitudes are decreased by $\frac{1}{30}$–$\frac{1}{40}$ times those obtained in the temperature increasing direction. Apparently, this irreversible conductivity behavior should correspond to the phase transition from β-phase to α-phase.

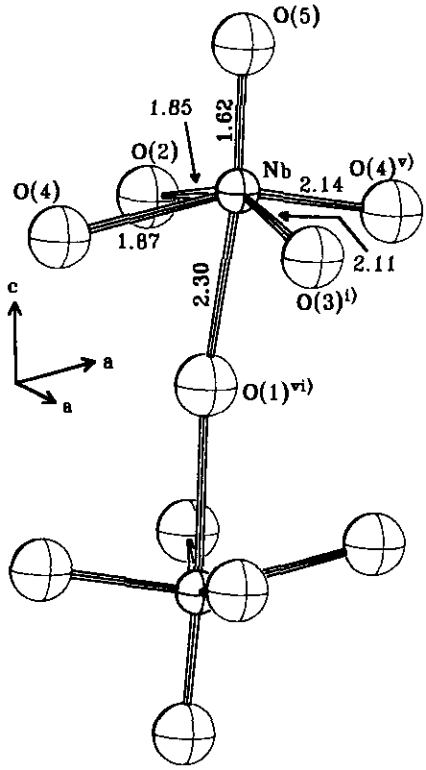

FIG. 6. Environment around niobium atoms in the β-phase of $AgLaNb_2O_7$.

As shown in Fig. 7, the tetrahedra neighboring by edge-sharing with the AgO_4 tetrahedra are all vacant for the β-phase, but are filled by silver atoms with 50% occupancy for the α-phase. The ionic motion of silver in this material should be restricted within the interlayer and take place at an adjacent site through the edge of the tetrahedra. In general, ionic conductivity σ and macro self-diffusion coefficient D are related to each other by the so-called Nernst–Einstein equation (25),

$$D = \frac{\sigma kT}{Nq^2},$$

where N is the concentration of mobile ions, k the Boltzmann constant, q the valence of mobile ions, and T the absolute temperature. If the ion conduction takes place by jump diffusion of the mobile ions through vacancies in the crystal, D is given by the following equation on the basis of the random walk process (*26*),

$$D = A\Gamma r^2,$$

where A is the constant concerned with the

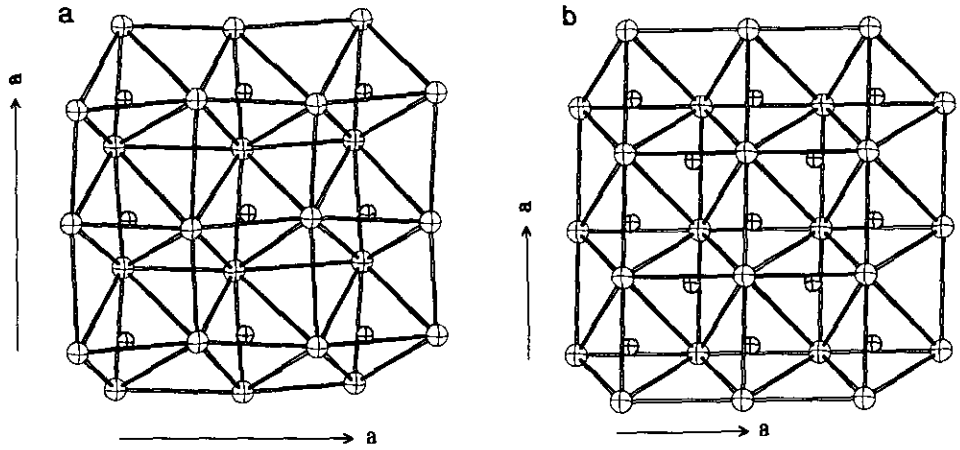

FIG. 7. AgO_4 tetrahedra linkage within the interlayer of β-phase (a) and α-phase (b) of $AgLaNb_2O_7$.

crystal structure, Γ the jump frequency, and r the distance between the neighboring sites for the ion jump. In $AgLaNb_2O_7$, A and r almost take the common values for the β-phase and the α-phase, respectively, due to their very close crystal structures. Therefore, the difference in ion conductive behavior between the two phases should be correlated with the difference in the degree of the frequency factor. Based on the simplest consideration, the frequency for the silver ion jump from an AgO_2 tetrahedron to an adjacent vacant tetrahedron in the β-phase could be twice as large as that in the α-phase because the probability for an adjacent tetrahedral site to become vacant is 50% due to the 50% occupancy for the site. It could be concluded that such a decrease in the diffusion coefficient for mobile silver ions accompanied by the phase transition leads to an abrupt decrease in the conductivity.

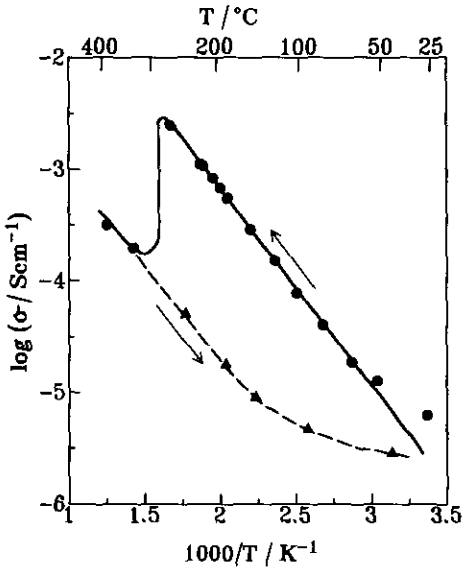

FIG. 8. Temperature dependence of conductivity for $AgLaNb_2O_7$ in both temperature-increasing and temperature-decreasing directions.

The values of ionic conductivity for pure $AgLaNb_2O_7$ are rather smaller than those for so-called fast ion conductors at any temperatures measured. The activation energy calculated from the slope of the log (σT) vs $1/T$ plot was found to be 38.0 kJ mol^{-1} in the temperature-increasing direction and 34.5 kJ mol^{-1} in the temperature-decreasing direction. These values are considerably higher than those for α-AgI (9.6 kJ mol^{-1}) (*27*) and $RbAg_4I_5$ (7.1 kJ mol^{-1}) (*28*), and are somewhat higher than that for the $AgI-Ag_2MoO_4$ glass ion conductor (~20 kJ mol^{-1}) (*29*). The reason for such poor ionic conduction being found in $AgLaNb_2O_7$ involving silver atoms with ionic character may be due to the fact that the site available for silver ionic conduction is only a tetrahe-

dral site, not any of the structures of the "average structure" responsible for fast ion conduction.

Acknowledgments

We are indebted to Mr. H. Minagawa for his help in data collection of the X-ray powder diffraction measurements and to Dr. M. Kitayama for her help in DTA and TGA measurements. The financial aid provided by Yamaguchi Foundation for Science and Technology is also gratefully acknowledged.

References

1. S. N. Ruddlesden and P. Popper, *Acta Crystallogr.* **10,** 538 (1957); **11,** 54 (1958).
2. M. Dion, M. Ganne, and M. Tournoux, *Mater. Res. Bull.* **16,** 1429 (1981).
3. M. Dion, M. Ganne, and M. Tournoux, *Rev. Chim. Miner.* **21,** 92 (1984).
4. A. J. Jacobson, J. T. Lewandowski, and J. W. Johnson, *J. Less-Common Met.* **116,** 137 (1986).
5. M. Gondrand and J.-C. Joubert, *Rev. Chim. Miner.* **24,** 33 (1987).
6. J. Gopalakrishnan and V. Bhat, *Inorg. Chem.* **26,** 4299 (1987).
7. M. M. J. Treacy, S. B. Rice, A. J. Jacobson, and J. T. Lewandowski, *Chem. Mater.* **2,** 279 (1990).
8. R. A. Mohan Ram and A. Clearfield, *J. Solid State Chem.* **94,** 45 (1991).
9. K. Domen, J. Yoshimura, T. Sekine, A. Tanaka, and T. Onishi, *Catal. Lett.* **4,** 339 (1990).
10. M. Sato, J. Abo, T. Jin, and M. Ohta, *Solid State Ionics* **51,** 85 (1992).
11. M. Sato, J. Abo, and T. Jin, *Solid State Ionics* **57,** 285 (1992).
12. M. Sato, J. Abo, T. Jin, and M. Ohta, *J. Alloys Comp.* (formerly *J. Less-Common Met.*), in press.
13. F. Izumi, *Nippon Kesshou Gakkaishi* **27,** 23 (1985).
14. Y. Takaki, T. Taniguchi, H. Yamaguchi, and N. Nakata, *J. Ceram. Soc. Jpn. (Int. Ed.)* **96,** 13 (1988).
15. D. H. Donney and H. M. Ondik, "Crystal Data Determinative Tables," Vol. 1, JCPDS, 1972.
16. D. B. Wiles and R. A. Young, *J. Appl. Crystallogr.* **14,** 149 (1981).
17. H. Toraya and F. Marumo, *Mineral. J.* **10,** 211 (1981).
18. J. A. McMillan, *J. Inorg. Nucl. Chem.* **13,** 28 (1960).
19. K. Yvon, A. Bezinge, P. Tissot, and P. Fischer, *J. Solid State Chem.* **65,** 225 (1986).
20. Von H. Hahn and C. De Lorent, *Z. Anorg. Allg. Chem.* **290,** 68 (1957).
21. S. Okamoto, S. I. Okamoto, and T. Ito, *Acta Crystallogr. B* **28,** 1774 (1972).
22. A. Rulmond, P. Tarte, G. Foumakoya, A. M. Fransolet, and J. Choisnet, *J. Solid State Chem.* **76,** 18 (1988).
23. M. L. Hackert and R. A. Jacobson, *J. Solid State Chem.* **3,** 364 (1971).
24. C. Wagner, "Proc. International Commission on Electrochemical and Thermodynamic Kinetics," Vol. 7, p. 361, 1957.
25. N. F. Mott and R. W. Gurney, "Electronic Processes in Ionic Crystals," Oxford Univ. Press, Oxford, 1940.
26. W. D. Kingery, H. K. Bowen, and D. R. Uhlmann, "Introduction to Ceramics," p. 223, Wiley, New York, 1976.
27. P. C. Allen and D. Lazarus, *Phys. Rev. B* **17,** 1913 (1978).
28. B. B. Owens and G. R. Argue, *J. Electrochem. Soc.* **117,** 898 (1970).
29. J. Kuwamoto and M. Kato, *Denki Kagaku* **46,** 356 (1978).